Inorganic Chemistry

Forum Article

pubs.acs.org/IC

What Can Density Functional Theory Tell Us about Artificial Catalytic Water Splitting?

Michael G. Mavros,[†] Takashi Tsuchimochi,[†] Tim Kowalczyk,[†,‡] Alexandra McIsaac,[†,§] Lee-Ping Wang,[†,⊥] and Troy Van Voorhis*[,†]

[†]Department of Chemistry, Massachusetts Institute of Technology, 77 Massachusetts Avenue, Cambridge, Massachusetts 02139 United States

[‡]Department of Chemistry, Nagoya University, Nagoya 464-8602, Japan

[§]Department of Chemistry, University of Chicago, 5735 South Ellis Avenue, Chicago, Ilinois 60637 United States

[⊥]Department of Chemistry, Stanford University, 318 Campus Drive West, Stanford, California 94305, United States

Supporting Information

ABSTRACT: Water splitting by artificial catalysts is a critical process in the production of hydrogen gas as an alternative fuel. In this paper, we examine the essential role of theoretical calculations, with particular focus on density functional theory (DFT), in understanding the water-splitting reaction on these catalysts. First, we present an overview of DFT thermochemical calculations on water-splitting catalysts, addressing how these calculations are adapted to condensed phases and room temperature. We show how DFT-derived chemical descriptors of reactivity can be surprisingly good estimators for reactive trends in water-splitting catalysts. Using this concept, we recover trends for bulk catalysts using simple model complexes for at least the first-row transition-metal oxides. Then, using the CoPi cobalt oxide catalyst as a case study, we examine the usefulness of simulation for predicting the kinetics of water splitting. We demonstrate that the appropriate treatment of solvent effects is critical for computing accurate redox potentials with DFT, which, in turn, determine the rate-limiting steps and electrochemical overpotentials. Finally, we examine the ability of DFT to predict mechanism, using ruthenium complexes as a focal point for discussion. Our discussion is intended to provide an overview of the current strengths and weaknesses of the state-of-the-art DFT methodologies for condensed-phase molecular simulation involving transition metals and also to guide future experiments and computations toward the understanding and development of novel water-splitting catalysts.

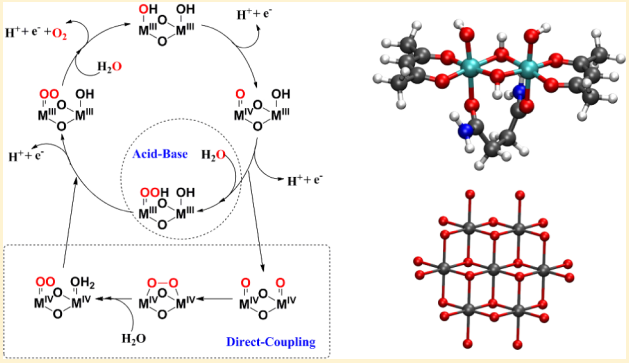

INTRODUCTION

An efficient and sustainable technology for the production of useful fuel from sustainable energy sources like the sun is the object of much contemporary scientific research across many disciplines. The first step in most solar energy conversion technologies is the absorption of sunlight by a chromophore;[1−3] however, electronic excitations are very short-lived, necessitating a mechanism for longer-term energy storage. One quite popular proposal is to store the solar energy in chemical bonds, using sunlight to split water and produce hydrogen gas as a fuel,

$$H_2O(l) \rightarrow H_2(g) + \frac{1}{2}O_2(g) \qquad E^\circ = 1.23\ V$$

where E° is reported with respect to the standard hydrogen electrode (SHE). This reaction can then be reversed, oxidizing hydrogen gas in a fuel cell to produce water. Artificial water splitting has received considerable attention recently, and several reviews discuss its significance and summarize challenges.[4,5] Effective catalyst designs range from small-molecule transition-metal complexes[6,7] to amorphous cobalt oxides[8] and perovskite materials,[9−11] operating under several different mechanisms. Progress toward higher efficiency hinges on a systematic understanding of the various water-splitting pathways, including the thermodynamic stability of various intermediates in the catalytic cycle and the kinetics of their interconversion.

At first glance, the thermodynamics of the water-splitting reaction seem quite simple. In one half-reaction, two molecules of water are split into four protons and a molecule of O_2, releasing four electrons at a potential of 1.23 V per electron with reference to the SHE. In the other half-reaction, which occurs at the SHE, two protons and two electrons combine to

Special Issue: Insights into Spectroscopy and Reactivity from Electronic Structure Theory

Received: January 31, 2014

   dx.doi.org/10.1021/ic5002557 | Inorg. Chem. XXXX, XXX, XXX−XXX

form one molecule of H_2. Nevertheless, the full catalytic cycle, illustrated schematically in Figure 1, involves several

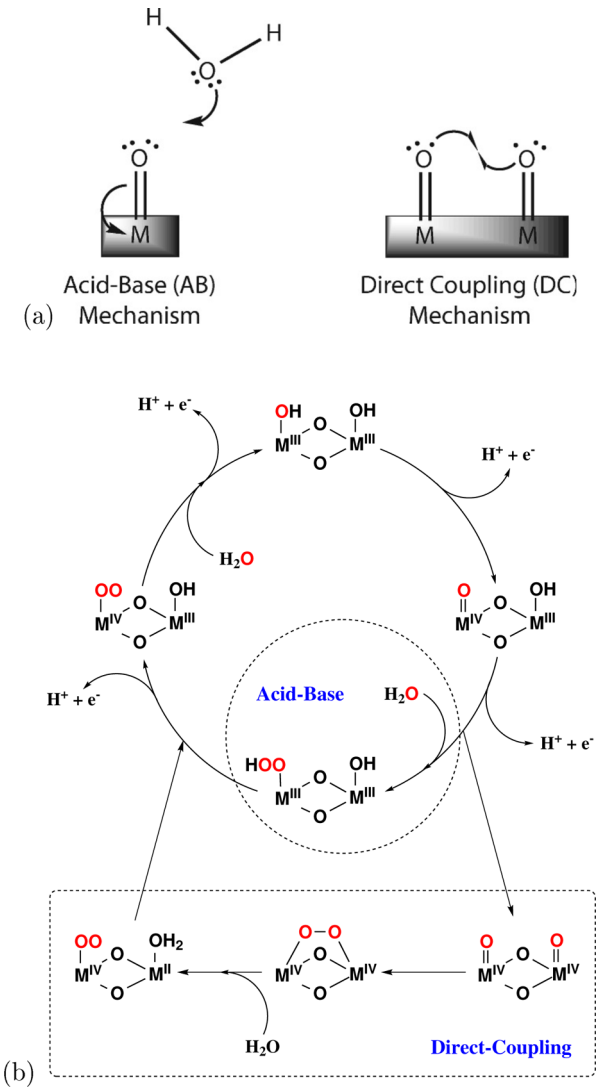

Figure 1. (a) Schematic pictures of the acid-base and direct (or radical)-coupling mechanism for oxygen evolution on a heterogeneous catalytic surface. Reprinted (adapted) with permission from ref 7. Copyright 2010 American Chemical Society. (b) Detailed breakdown of the two mechanisms. In accordance with the observations of many in the literature,[12,13] we focus only on mechanisms involving a Lewis acid, which is thought to be essential for oxygen evolution to occur.

intermediates whose thermodynamic stabilities and interconversion kinetics dictate the overall catalytic activity. Furthermore, the stability of certain intermediates necessitates voltages larger than 1.23 V (overpotential) when the water-splitting reaction is run on a catalytic surface. Ultimately, the catalyst's molecular structure and experimental conditions determine the observed efficiency through four interrelated factors: (i) thermodynamics of stable intermediates; (ii) solvent effects; (iii) kinetics of chemical and electrochemical steps; and (iv) mechanisms of O−O bond formation and O_2 release.

The catalytic cycle proceeds through a series of stable intermediates, leading up to the central event of water splitting: formation of the O−O bond in the oxygen evolution reaction (OER). Two qualitatively different mechanisms, dubbed the "acid-base mechanism" and "direct-coupling mechanism" (or "radical-coupling mechanism"), are shown schematically in Figure 1a and in more detail in Figure 1b. The acid-base mechanism proposes that the O−O bond is formed via a nucleophilic attack on an electrophilic metal oxo species; it is suspected to be the mechanism at play for oxygen evolution in a wealth of synthetic systems.[7,14,15] By contrast, the direct-coupling mechanism proposes that two high-valent metal oxo species on the catalytic surface come together to form O_2; recent computational[16] and experimental[17,18] evidence suggests that this mechanism may be at play for certain metal oxide catalysts.

The acting mechanism for O−O bond formation depends on the participating transition-metal center(s)[19] and pH,[20] among other factors. Further complicating matters, the relationship between OER thermodynamics and kinetics is not always clear. Many of the reactive steps shown in Figure 1b are proton-coupled electron-transfer (PCET) events whose nature (concerted vs sequential) depends on the transition-metal system.[6,14,16−18,21,22] Additionally, the critical O−O bond formation step is, invariably, a chemical step—one that depends little on the governing electrical potential and highly on small fluctuations of the local environment. The aqueous environment plays a critical role here, both in providing the proper electrostatic environment around the metal oxo species to facilitate the reaction, and also as a reactant itself: water ultimately is responsible for the displacement of O_2 from the catalyst.

The role of computation in understanding heterogeneous catalysis cannot be overstated. With appropriate care and for systems of moderate size (up to hundreds of atoms), density functional theory (DFT) calculations in particular can be used to make useful predictions about the thermodynamics, kinetics, and mechanism of the water-splitting reaction on a wide variety of materials, saving time and money in the laboratory by suggesting experiments that should be performed. In particular, DFT can, in principle, be used both to screen large numbers of catalytic materials[23] and to provide a detailed understanding of the catalytic process on a particular material,[16] both of which can be utilized to guide experimentation. While computation is poised to provide important insight, black-box application of DFT to the problem could easily lead to false conclusions. Proper care must be taken in order to extract accurate thermodynamic data and meaningful trends from electronic structure calculations.

In this Forum Article, we review the role of computation in understanding water splitting by artificial transition-metal catalysts. We first review what DFT is particularly good at: thermochemistry. We focus particularly on approaches utilizing so-called chemical descriptors of catalytic activity to form volcano plots, an extension of the established technique of Sabatier analysis[24] to the age of supercomputers.[25] We then examine high-fidelity simulations of catalytic water splitting, in which the treatment of solvation and the selection of model catalysts are key factors. We pay particularly close attention to the kinetics of PCET events so ubiquitous in this reaction. Finally, we examine in detail factors relating to the determination of mechanism from simulation, focusing on ruthenium catalysts as a case study. Our hope is that we may provide a concise summary of the state-of-the-art methods and best practices for applying DFT to study catalysis in order to guide future work.

dx.doi.org/10.1021/ic5002557 | Inorg. Chem. XXXX, XXX, XXX−XXX

COMPUTATIONAL THERMODYNAMICS OF WATER SPLITTING

Water-splitting catalysis is not a concerted process but proceeds through stable intermediates. To know the intermediates in the water-splitting cycle, we must first propose a mechanism. Once we propose a mechanism and enumerate the intermediates, we can calculate the thermodynamic stability of the different intermediates and determine how stable they are in relation to one another. The thermodynamic stability of different intermediates in the catalytic cycle depends heavily on both the nature of the catalytic surface (both the type of transition metal and uniformity) and the catalytic mechanism. This concept is shown graphically in Figure 2: although the *overall* reaction may have a potential of 1.23 V per electron transferred, *individual* reaction steps may have potentials thermodynamically uphill by a value much greater than 1.23 V (or even downhill!).

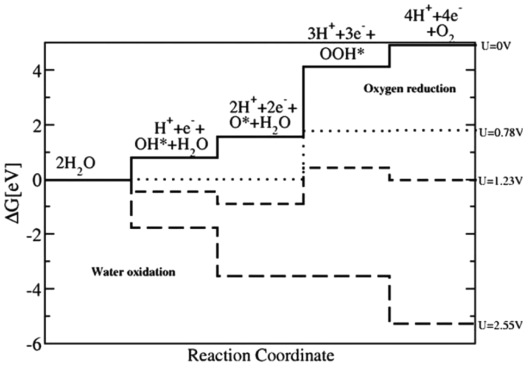

Figure 2. Thermodynamic stability of intermediates in the water-splitting reaction, assuming an acid-base mechanism and fast PCET events. The thermodynamic stability of the intermediates changes as one applies an electrochemical bias voltage. An asterisk (*) denotes a species bound to a transition-metal surface. The specific system under study in this investigation is OER on a Pt(111) surface, but the underlying analysis applies universally to other bulk and molecular water-splitting catalysts. Reprinted with permission from ref 38. Copyright 2005 Elsevier.

There are also reaction barriers between these steps, which determine the kinetics of electron transfer. The overpotential of the overall reaction depends on the magnitude of the largest barrier in the entire cycle. If we ignore the activation energy (and thus reaction kinetics) by assuming that it is small, then the overpotential of a given mechanism is determined entirely by thermodynamics. This overpotential will be an underestimate of the true overpotential but can be quite a useful estimate and is attainable without studying the reaction kinetics in detail. In certain cases, ignoring barrier heights is justifiable: for example, PCET events, ubiquitous in water splitting, usually have small barriers, and PCET rate constants often contain large quantum-mechanical tunneling prefactors.[26,27] In other cases—cases that we will examine in detail later—it is not as justifiable, and a careful treatment of the reaction barriers is necessary.

Thermodynamics Overview. DFT is quite well-suited for computing the relative thermodynamic stabilities among a series of compounds. Using reasonably sized basis sets and hybrid functionals, one can get very close to "chemically accurate" heats of atomization (and, with suitable use of experimental tables, heats of formation) for compounds in the gas phase at 0 K.[28,29] The challenges of DFT thermochemistry come with the prediction of free energies of formation in solution at finite temperature. For ease of notation, we shall illustrate how to compute free energies of formation at 298 K, but in practice this protocol can be applied for any temperature. Fortunately, there has been much development on this topic in recent years;[30−34] we shall summarize some of the main findings here.

Many authors have made use of thermodynamic cycles in order to study the thermodynamics of water splitting. Yang and Baik have developed computational methods for studying the thermodynamics of water splitting from a molecular perspective;[35−37] likewise, Nørskov et al. pioneered similar methods for plane-wave computations on simulated surfaces.[38,39] In this paper, we shall focus in particular on one example of a protocol, shown in Figure 3. This particular protocol is not original or unique but is chosen in order to clearly illustrate themes in water-splitting thermodynamics, which are detailed below.

The cycle in Figure 3 can be used to calculate $\Delta G^{298}_{f,aq}$, from which reaction free energies—and thus redox potentials—can be computed. Many ideas in this cycle are well-established for wave-function-based methods[28,29,40] and have more recently been extended to DFT methods.[41] The main idea can be summarized as follows:

1. Computation of the atomization energies from DFT is straightforward, but computation of the formation energies is not. We must thus first adjust the "reference" from elements in their

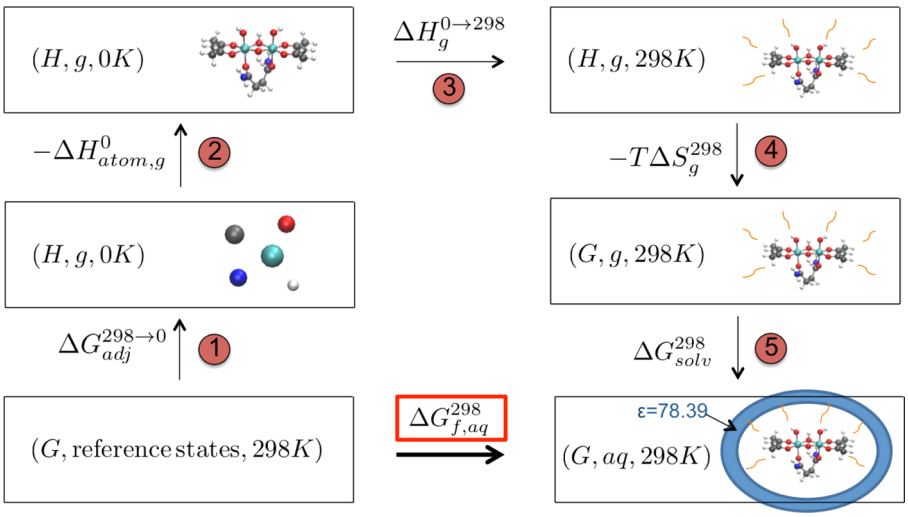

Figure 3. Thermodynamic cycle that can be used for the computation of $\Delta G^{298}_{f,aq}$, the aqueous free energy of formation of a molecule. The numbered steps correspond to the numbered steps in the main text. Once one references the absolute energy of a molecule to a suitable standard state (steps 1 and 2 in the cycle), one can then apply a series of corrections to the DFT-calculated internal energy to adjust the temperature from 0 K to an arbitrary temperature (step 3; here, room temperature, or 298 K), include entropic effects due to molecular vibrations (step 4), and include the effects of solvent electrostatics (including those on entropy) through a continuum dielectric model (step 5).

dx.doi.org/10.1021/ic5002557 | Inorg. Chem. XXXX, XXX, XXX−XXX

standard state at 298 K to atoms at 0 K using empirical data from standard thermodynamic tables[42] by applying an adjustment $\Delta G^{0\rightarrow 298}_{adj}$. This will eventually allow for calculation of the free energies of formation.

2. Compute $\Delta H^{0}_{atom,g}$, the gas-phase atomization energy at 0 K, from the DFT energies of the compound of interest and its constituent atoms.

3. Compute the vibrational frequencies of the molecule using a harmonic frequency analysis; from this, extract (a) $\Delta\Delta H^{0\rightarrow 298}_{f,g} = \Delta\Delta H_{vib} + \Delta\Delta H_{rot} + \Delta\Delta H_{trans} + PV = {}^{1}/_{2}\sum_i \hbar\omega_i \coth(\hbar\omega_i/2RT) + {}^{3}/_{2}RT + {}^{3}/_{2}RT + RT$ (note that this includes the zero-point vibrational energy, as well as thermal contributions from higher vibrational states within the harmonic approximation; the translational and rotational contributions to the enthalpy are treated classically) and (b) $T\Delta S^{298}_{g} = \sum_i[\hbar\omega_i \coth(\hbar\omega_i/2RT)]/2 + RT \ln[{}^{1}/_{2}\ \mathrm{csch}(\hbar\omega_i/2RT)]$. This comes from the standard statistical mechanical relationship for vibrational enthalpy.

4. Compute $\Delta G^{298}_{f,g} = \Delta H^{0}_{atom,g} + \Delta G^{0\rightarrow 298}_{adj} + \Delta\Delta H^{0\rightarrow 298}_{f,g} - T\Delta S^{298}_{g}$, the gas-phase free energy of formation of the molecule at 298 K.

5. Compute ΔG^{298}_{solv}; then $\Delta G^{298}_{f,aq} = \Delta G_{f,g} + \Delta G^{298}_{solv}$.

In passing, we will note that the computation of $\Delta H^{0}_{atom,g}$ can be nontrivial for transition metals, as the ground-state spin multiplicity is often incorrectly predicted by DFT.[43,45] Procedures have been tested to get the ordering of the spin states correct and minimize the errors in Δ_o, the octahedral crystal-field-energy spin splitting.[46,47]

Furthermore, computation of ΔG^{298}_{solv} is a delicate matter. In a continuum dielectric solvation calculation, the molecule of interest is enclosed in a cavity; then ,the rest of the space is filled with a dielectric medium. The medium is allowed to polarize the electrons on the molecule (and vice versa) in a self-consistent fashion, which ultimately influences the total energy of the system. Accurate solvation free energies rely largely on the quality of the cavity used as well as the parametrization of the dielectric response of the polarized continuum. Many models capture these effects with different underlying physics, each with their own strengths and weaknesses; for a good review on the topic, we direct interested readers to the exchange in refs 33 and 48.

From $\Delta G^{298}_{f,aq}$, we can easily compute a reaction free energy, ΔG^{298}_{r}, from which we can calculate an absolute electrochemical potential

$$E^{\circ} = -\frac{\Delta G^{298}_{r}}{nF}$$

where n is the number of electrons transferred and F is the Faraday constant. One final step must be completed before a comparison to experiment is possible: adjusting the absolute potential with respect to a reference electrode. Experimentally, redox potentials are measured with respect to a reference electrode or an internal standard reference redox couple whose absolute potential is known. Computationally, redox potentials are often calculated as the difference in (free) energy between a species with an excess electron and that same species without its excess electron. In order to compare theory to experiment, these two methods must be reconciled.

One complication that arises in these calculations is how to treat the solvation of a proton and an electron in order to get accurate free energies. The solvation free energy of both of these particles is beyond the reach of the state-of-the-art methods in computational chemistry; as such, alternatives must be used. One common approach is to compute an absolute free energy of solvation for each by using an experimental reference value.[49−51]

Another common approach that we use in our calculations is a *computational internal standard* (see, e.g., refs 38 and 52). As an example, consider the PCET reaction

$$MH^{2+} \rightarrow M^{3+} + H^{+} + e^{-}$$

If we assume that the reaction

$$H^{+} + e^{-} \rightleftarrows \frac{1}{2}H_2$$

is in equilibrium (E° = 0.00 V), then we can add the two reactions of interest without changing the redox potential of the reaction of interest and compute the absolute redox potential of

$$MH^{2+} \rightarrow M^{3+} + \frac{1}{2}H_2$$

In doing so, we have used a computational internal standard; namely, we have referenced all of our redox potentials to the redox potential of the atomization of molecular hydrogen. This specific choice of a reference redox couple is given a special name in the experimental literature: the SHE. In principle, this referencing technique can be applied to *any* redox couple; besides referencing to the SHE, referencing to the ferrocene couple has been quite popular in recent years.[52] In practice, it is most convenient to compute the redox potential of a reaction with respect to a reference that is easily experimentally accessible.

Application to the First-Row Transition-Metal Series. In order to illustrate the utility of the procedure described in the previous section, we applied the thermodynamic protocol outlined above to compute the overpotential for water splitting on a family of model molecular catalysts, shown in Figure 4a, spanning the first row of the transition-metal series. The selection and design of the model catalysts are discussed in the Supporting Information. Figure 4b shows our results, where we plot the activity versus our descriptor, the atomic number of the transition-metal center. Both the acid-base mechanism

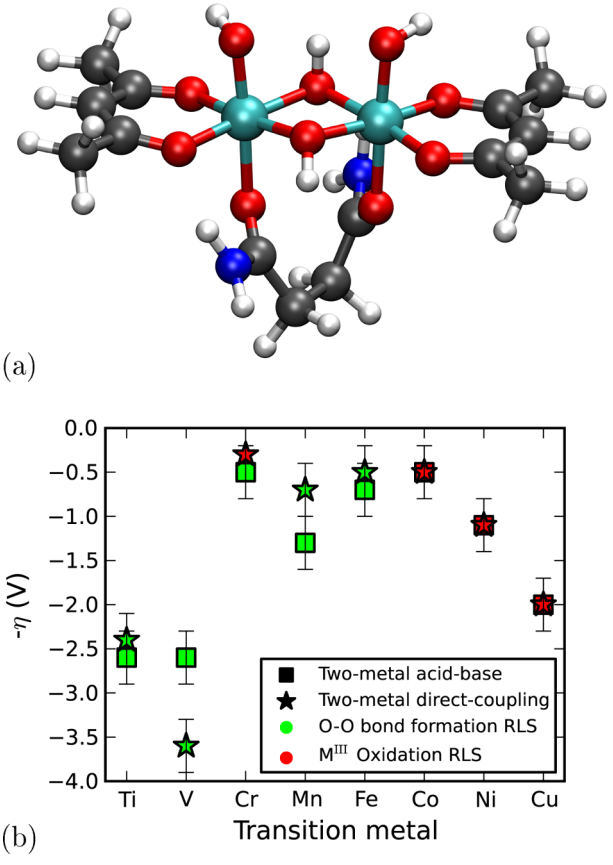

Figure 4. (a) Model transition-metal oxide "surface". Transition-metal atoms are displayed as cyan, and the redox-active sites are connected axially to the transition-metal centers. Transition-metal oxidation states are permuted by changing the protonation state of the redox-active site. (b) Lower bound on the negative overpotential (η) as a function of the transition-metal identity. Error bars represent the intrinsic error of DFT calculations on these sorts of systems, estimated generously as ±0.3 V.[44] Note the change in the RLS, regardless of the mechanism, as one transitions from the left half of the periodic table to the right half.

dx.doi.org/10.1021/ic5002557 | Inorg. Chem. XXXX, XXX, XXX−XXX

and direct-coupling mechanism are considered. In order to calculate an overpotential for the direct-coupling mechanism, the two chemical steps must be grouped with an electrochemical step. We performed the grouping as follows: (i) if a chemical step is downhill, assume that the previous step is preequilibrium; group the chemical step with the previous step; (ii) if a chemical step is uphill, it is rate-determining for the chemical transformation; group it and all other following chemical steps with the next electrochemical step.

As Figure 4 shows, the lower bound on the overpotentials that we calculate using our model system has two linear regions, which intersect at a peak of activity. This trend has been observed generally for many molecular scaffolds, as explained in more detail below. Our data also serve as a scan across the first period of the periodic table for catalytic activity and its relationship to mechanism. There are two interesting points to note: (i) the observed activity does not depend on the mechanism to within the error of our calculations; (ii) the rate-limiting step (RLS) of the OER shifts from O−O bond formation to the formation of M^{IV} from M^{III} on going from left to right across the period.

The first point raises a bit of a conundrum because the rate of oxygen evolution *should* depend on the mechanism provided the RLS is O−O bond formation. This dependence is not observed. Regardless, the fact that the overpotentials do not vary with the mechanism can be classified as a strength of this type of thermodynamic analysis because one can predict overpotentials without worrying about getting precisely the correct mechanism. As a caveat, the converse is not true: just because the overpotential agrees with an experimentally observed value does not mean that the mechanism that is used to predict the overpotential is correct. Thermodynamic analysis is incredibly useful as a fast, computationally cheap screen of a large number of potential catalysts, but conclusions about the mechanism or the chemical nature of oxygen evolution cannot and should not be drawn from such an analysis.

Chemical Descriptors of Reactivity. In the previous two sections, we described computation of the thermodynamics of the water-splitting reaction on a heterogeneous catalyst and demonstrated how thermodynamics can be used as a predictor of the catalytic activity; we will now review the theoretical work that went into pioneering this approach and the experimental work that has grown from it. Much of the initial work in this area came out of the group of Nørskov,[25,38,39,53,54] but other theoretical groups[55,56] and some experimental groups[9,57] have extended the principles and used them to explain experimental observations. We do not plan on engaging in a comprehensive review of transition-metal water oxidation catalysis here; for such a review, the interested reader is directed to ref 58.

The use of thermodynamics to describe catalysis is not a new concept: Sabatier introduced his eponymous principle in 1911.[24] The Sabatier Principle states that the optimal catalyst for a particular substrate will not bind the substrate too weakly (because if it did, the substrate would not bind to the catalyst) or the product too strongly (because if it did, the product would never be released from the catalytic surface, and the catalyst would be "poisoned"). As a special case of the discussion in the previous section, Sabatier analysis suggests that it should be possible to use thermodynamics alone to predict the catalytic activity.

Nørskov extended this analysis to the 21st century by proposing that one could computationally screen a large number of catalysts using DFT by focusing on the metal−oxygen bond strength. By the Sabatier Principle, the perfect catalyst for water splitting should bind water "strongly" and oxygen "not too strongly"; because both bind through a metal−oxygen bond, a plot of the catalytic activity as a function of the metal−oxygen bond strength should have a maximum at the "optimal" metal−oxygen bond strength. In practice, one forms two calibration curves (one with a positive slope and one with a negative slope) by calculating the metal−oxygen bond strength of a large number of species and correlating these with experimentally measured activities; these two calibration curves form a "volcano" of activity, with their intersection lying at the peak of the volcano. Then, one can screen large numbers of compounds computationally, and those compounds with metal−oxygen bond strengths near the peak of the volcano are predicted to have high catalytic activity.

The metal−oxygen bond strength is not the only useful chemical descriptor for Sabatier analysis. Other descriptors exist as well, including the filling of transition-metal e_g orbitals—the orbitals most implicated in surface metal−oxygen bonds. Ultimately, these all boil down to the same sort of Sabatier Principle: if it is easy for the substrate to form a chemical bond to the catalyst and easy for the product to break a chemical bond with the catalyst, the catalyst will work well. Remarkably, these volcano plots work extremely well at predicting the activity as a function of a simple chemical descriptor. Figure 5 displays volcano plots for several different chemical descriptors, showing that this correlation is not fictitious.

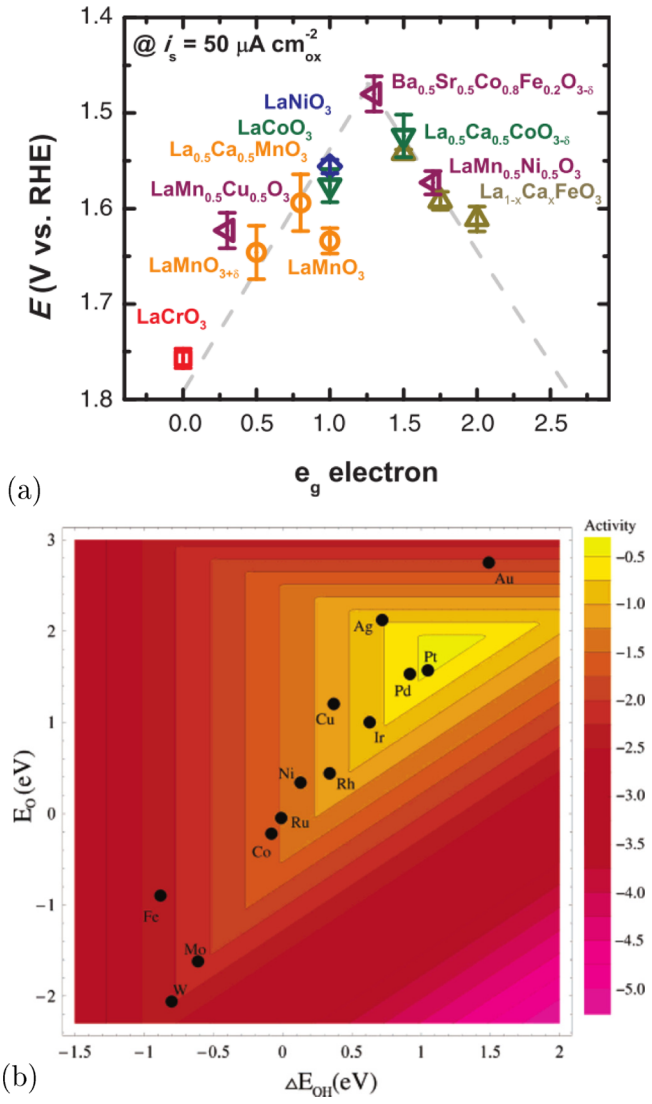

Figure 5. Sample volcano plots using (a) e_g orbital occupation (Reprinted with permission from ref 9. Copyright 2011 AAAS) and (b) cross-correlation of the metal OH/metal O binding energy as a chemical descriptor (Reprinted with permission from ref 39. Copyright 2004 American Chemical Society).

One major criticism of this Sabatier-type analysis is that it assumes that the RLS of catalytic water splitting is either the association of the substrate with the catalyst or the dissociation of the product from the catalyst. In many cases, this is simply not true: redox steps and O−O bond formation have been found to be rate-limiting in certain systems.[7,10,16−18,59−62] Sabatier analysis is thus successful when the RLS of the catalytic cycle is a redox step, but its scope is limited to

dx.doi.org/10.1021/ic5002557 | Inorg. Chem. XXXX, XXX, XXX−XXX

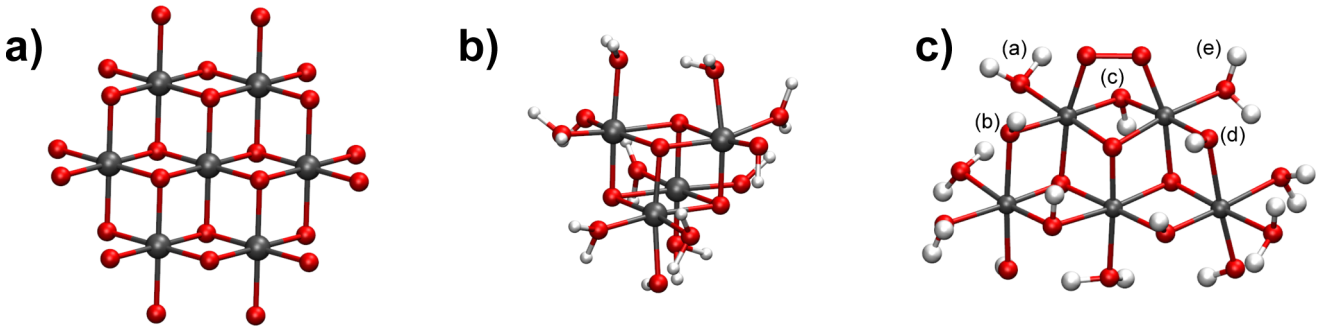

Figure 6. (a) Seven-center model of the CoPi surface (protons omitted), consisting of edge-sharing CoO_6 octahedra and supported by EXAFS studies. (b) Cubane Co_4O_4 model of the CoPi catalyst, used in ref 16. (c) O−O bonding in the five-center CoPi model, which was used for the additional calculations described in this work. Letters identify terminal oxo (a and e) and bridging μ-oxo (b−d) protons available for abstraction in the third and fourth PCET events.

such systems; as such, the use of Sabatier analysis is often precluded when the RLS of a catalytic cycle is not known ahead of time. Nevertheless, the technique is powerful, in that it uses *thermodynamic* information (along with an assumption about the RLS of the cycle) in order to predict *kinetics*.

■ MODELING WATER-SPLITTING KINETICS

DFT thermochemistry can often reproduce trends in the catalytic activity, as illustrated by the volcano plot analysis in the previous section. This level of modeling can provide actionable insight without a detailed understanding of the mechanism of catalytic activity. However, to determine plausible reaction pathways or to predict the activity of novel catalyst designs, a mechanistic understanding of the catalytic cycle is indispensable. Strictly thermochemical approaches neglect the role of kinetics, which must be incorporated into the simulation strategy for mechanistic studies. In this section, using recent computational studies of Nocera's CoPi cobalt oxide catalyst[8,17,63,64] as a basis for discussion, we discuss computation of redox potentials in solution and the insight it can provide into the kinetics of catalytic water splitting.

Catalyst Model Selection. The active form of the aqueous CoPi catalyst is a cobalt oxide cluster possessing pendant water and hydroxo ligands. The catalytic cycle of CoPi is comprised of a series of four oxidations of the CoPi−water complex coupled to formation of an O−O bond, release of O_2 from the catalytic surface, and regeneration of the catalyst resting state by water addition.[16] Identification of the rate-determining step (RDS) of the CoPi catalytic cycle is a central goal of computational studies. The RDS controls the turnover rate, and its identification helps to narrow the range of plausible mechanisms. For chemical (bond-breaking and forming) steps in the cycle, the activation free energy $\Delta G^{\ddagger}$ is the key quantity to be determined, while for redox events, the electron-transfer kinetics are governed predominantly by the redox potentials of the catalyst.

Given the extensive network of single-step chemical reactions that can take place in, on, and around the CoPi catalyst, an exhaustive exploration of all possible water oxidation pathways is possible only for model systems of modest size. EXAFS studies support structures as small as the seven-center cobaltate model[65] shown in Figure 6a, but initial mechanistic studies of the CoPi catalyst focused on a minimal four-center cubane model (Figure 6c). This model permits quantification of both acid-base and direct-coupling mechanisms while satisfying Occam's razor by limiting the investigation to the simplest mechanism capable of explaining experimentally observed features.

To consider additional PCET pathways not testable with the cubane model, we introduced a five-center model (Figure 6b), shown here in the state immediately following two PCET events and O−O bond formation. Here, terminal oxo (labels a and e) and μ-oxo (labels b−d) protons are both available for abstraction by PCET. The five-center model is thus capable of distinguishing among a larger variety of PCET pathways.

A related study of water splitting on CoPi[66] raised the important issue of identifying the lowest-energy protonation state of the model complex. Using a computational model different from the one used in ref 16, Li et al. found a lower-energy protonation state for the four-center catalyst, containing protonated μ-oxo bridges. DFT molecular dynamics (MD) simulations of representative Co_6O_{23}, Co_7O_{24}, and Co_7O_{26} clusters by Mattioli et al. also suggested a role for protonated μ-oxo atoms in the resting state.[67] Their model structures were derived from the known crystal structure of $LiCoO_2$ and included a linked pair of perfect Co_4O_4 cubanes, a pair of defective cubanes (identical to the seven-center model discussed above), and a mixed case. The structural differences in these studies lead to differing conclusions about the O−O bonding mechanism in CoPi, as discussed below.

Solvent Effects. In practice, DFT-derived reduction potentials can depend strongly on the level of theory at which the solvent is treated, especially for protic solvents like water. This dependence has been investigated by us[34] and others,[33,68,69] supporting an informed decision about how to model the aqueous environment of the CoPi catalyst. The two fundamentally different approaches to modeling this environment are implicit (or continuum) and explicit (or atomistic) solvation models. In the former, the solute density responds self-consistently to a surrounding dielectric continuum parametrized according to the identity of the solvent. This is a mean-field treatment of solvation in which solute flexibility can be described, in principle, through conformational sampling but is often only accounted for within the harmonic approximation. Atomistic treatment of the solvent removes most of these approximations but also requires extensive configurational sampling to incorporate all solute and solvent degrees of freedom. As a consequence, modeling with an explicit solvent is much more computationally demanding, and one must often tolerate a limited sampling of solvent configurations or a more approximate description of the solvent electronic structure. It is possible to combine the strengths of both methods through

dx.doi.org/10.1021/ic5002557 | *Inorg. Chem.* XXXX, XXX, XXX−XXX

three-layer models such as a quantum mechanics/molecular mechanics/polarizable continuum model (QM/MM/PCM) strategy.[70] Semiempirical and polarizable molecular mechanics (MMpol) models, which lie between the quantum and classical approaches in complexity, offer additional flexibility in constructing multilevel strategies.[71,72] There are also approaches that do not easily fit into the implicit versus explicit solvation paradigm, such as the reference interaction site model (RISM) approach.[73,74]

The CoPi water oxidation studies of Li et al.[66] employed a Poisson–Boltzmann implicit solvent model,[75] based on the success of this approach for modeling biological water oxidation.[12] However, in the case of water oxidation by the CoPi catalyst, the potentially important role of hydrogen bonding at the surface of the catalyst is a strong argument against the use of implicit solvation models, which do not account for hydrogen bonding across the artificial solute–solvent interface.

In a benchmark study of reduction potentials of aqueous transition-metal clusters, we showed that DFT (using the B3LYP functional)[76] with the conductor-like screening model (COSMO)[77] successfully predicts the experimental reduction potentials for organic molecules, metallocene complexes, and transition-metal complexes in various solvents, with the key exception of octahedrally coordinated aqueous transition-metal complexes.[34] Figure 7 illustrates this trend: the calculated

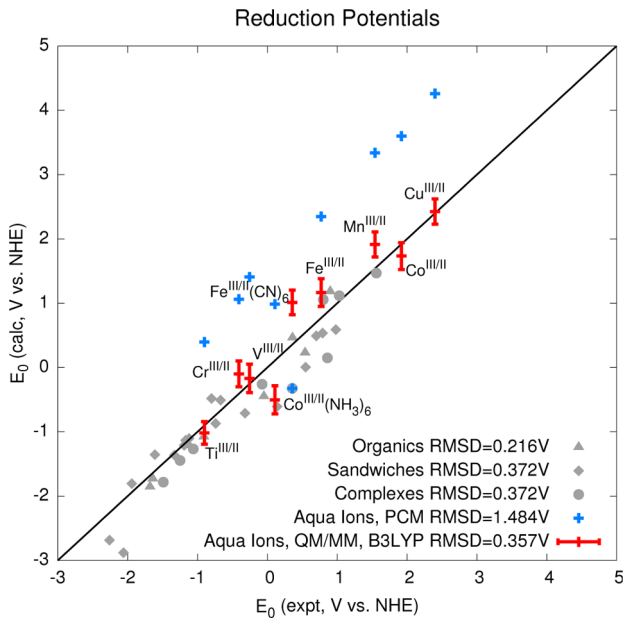

Figure 7. Comparison of the calculated and experimental reduction potentials $E°$ (eV). Reprinted with permission from ref 34. Copyright 2012 American Chemical Society.

reduction potentials of aqueous transition-metal complexes, shown in blue, are nearly all overestimated by more than 1 V, in contrast to root-mean-square deviations (RMSDs) of 0.2–0.4 V between the calculated and experimental reduction potentials for all other classes of complexes. A polarizable QM/MM (QM/MMpol) treatment showed significant improvement, achieving an RMSD similar to those of the other systems in an implicit solvent. In the QM/MMpol model, electronic polarization of the solvent due to redox events was accounted for explicitly;[72] its inclusion proved to be essential for reproducing the experimental reduction potentials. The QM/MMpol approach overcomes the failures of implicit solvation for aqueous transition-metal complexes but at significant computational cost. By isolating the effects of solute flexibility and of temporal solute–solvent correlation on the solvation energy, we showed that hydrogen-bonding effects are the primary feature absent from the implicit solvation models, which account for most of the error in the calculated reduction potentials.

The CoPi studies of Mattioli et al. also rely on an explicit representation of the solvent, treating the surrounding water at the same DFT level of theory as the catalyst itself.[67,78] This even-handed approach accounts for hydrogen-bonding effects—to the extent that the underlying functional successfully describes noncovalent interactions—while naturally including both electronic and orientational polarization of the solvent after a redox event. The only clear disadvantage of such an approach is computational cost. In the next section, we will explore how the model selection and solvent considerations above influence the calculation of redox potentials and reaction profiles for water oxidation in CoPi.

Redox Potentials for the CoPi Catalyst. In previous work, we showed a direct-coupling pathway for O–O bond formation on the four-center CoPi model of Figure 6b, where an O–O bond formed spontaneously between a pair of terminal oxo ligands after two PCET events.[16] The redox potentials for these two PCETs, computed using the QM/MMpol approach described in the previous section, are 0.8 and 1.4 V, respectively. Here we report redox potentials for the third and fourth PCET events, assuming that both take place before water addition and O_2 displacement. The same QM/MMpol strategy as that used for the first two PCET events is employed here: the QM region consists of the CoPi model complex including all hydroxyl and water ligands, surrounded by water treated through the MMpol model. Redox potentials were obtained through conformational sampling of the ionization potential and electron affinity of the catalyst in different oxidation states, as described in the Supporting Information. All possible pairs of deprotonation sites, indicated in Figure 6c, were considered.

The pathway with the lowest determined overpotential consisted of deprotonation of a water ligand (a) at 0.2 V, followed by deprotonation at a μ-oxo site (b) at 1.2 V; the complete series of redox events is summarized in Figure 8. For the fourth PCET, deprotonation of a second water (e) was calculated to require an additional potential of 0.4 V above the (a and b) pathway. Interligand proton transfer on CoPi is also relatively facile in the simulations, evidenced, for example, by proton transfer from water to a hydroxyo ligand preceding the fourth PCET in Figure 8. The simulations show a lower redox potential for the fourth PCET than for the second PCET preceding O–O bond formation. Therefore, it is feasible for all four PCET steps to precede water addition, making O_2 release a plausible RLS. This finding helps to rationalize the Sabatier-type analysis discussed previously by supporting its underlying assumption that the RLS is a catalyst–reactant association or dissociation process.

The prediction of water-splitting kinetics in catalysts like CoPi ultimately hinges on three capabilities: simulating solvent dynamics, accurately computing redox potentials, and estimating reaction free-energy barriers. The computational investigations presented here each addressed these requirements in slightly different ways, but they collectively point to several

dx.doi.org/10.1021/ic5002557 | Inorg. Chem. XXXX, XXX, XXX–XXX

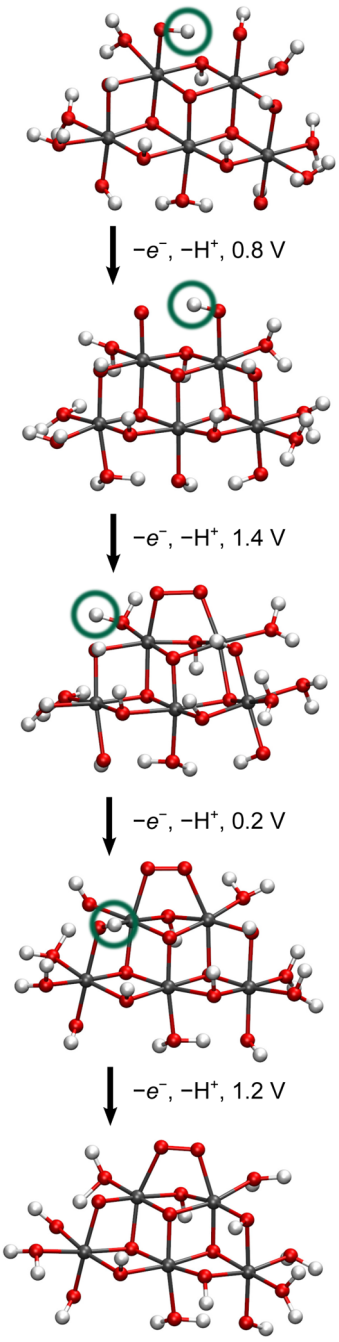

Figure 8. Oxidations and bond rearrangements on CoPi leading up to water addition and O_2 release, assuming a direct-coupling mechanism across neighboring terminal oxos. The lowest redox potential identified for each step is shown with the corresponding deprotonation site.

points of consensus about CoPi. Mattioli et al. carried out direct Car−Parrinello MD (CPMD) simulations of a solvated CoPi complex including full DFT treatment of water. Redox processes were simulated by removing electrons at fixed time intervals of 1 ps.[78] The time scale is incompatible with the relaxation time of water[79] but allowed for real-time simulation of the full sequence of redox events within DFT. The simulations did not show spontaneous formation of terminal Co(O) groups until all four electrons were removed, requiring an overpotential of 1.87 V for a Co_6O_{23} model catalyst. Li et al. considered redox events on the cubane Co_4O_4 model using an implicit solvent and found a slightly lower barrier for water attack than for direct coupling after the first two oxidations.[66]

All of the studies agree that the four-center model for CoPi cannot fully account for all experimental observations, especially the distribution of bond lengths determined by X-ray absorption spectroscopy. Regarding the sequence of redox processes, the QM/MM and CPMD studies agree on several points: (1) O−O bonding can proceed after the loss of as few as two electrons, although losing additional electrons helps; (2) preequilibrium steps involving proton transfer are likely because intramolecular proton transfer is facile on the surface of CoPi; (3) direct coupling, not an acid-base mechanism, is responsible for O−O bonding in the Co_4O_4 model cluster. It is, of course, possible that multiple mechanisms contribute to the overall performance of a heterogeneous, self-assembled catalyst such as CoPi.

The direct-coupling mechanism supported by the QM/MM and CPMD studies is at odds with the implicit solvation study of Li et al., where O−O bonding occurred between an oxo group and an attacking water molecule. This difference underscores the importance of treating catalyst−solvent interactions explicitly in order to accurately model catalytic water oxidation. For this reason, progress in the theoretical modeling of water oxidation is closely linked to the broader challenge of developing high-quality theoretical models for water and its interactions with solutes.

PREDICTING THE MECHANISM OF WATER SPLITTING

We now direct our attention to how one predicts the mechanism of water splitting on catalytic surfaces. In water oxidation catalysts, PCET is key because it significantly compensates for the high redox potential of electron transfer. However, not all of the catalytic reaction steps go through PCET, and identifying the correct reaction pathway remains an open question in many cases: is the mechanism based on acid-base or direct coupling? What is the key step for O−O bond formation? Knowing the detailed mechanism of water oxidation is crucial to understanding and systematically improving catalysts. Computationally, it is essential to obtain accurate redox potentials to evaluate a proposed mechanism. Here we take a series of ruthenium complexes as an example to showcase recent research aiming to propose catalytic mechanisms using DFT.

Acid-Base Mechanism. In contrast to CoPi, where direct coupling is currently the favored reaction mechanism, the acid-base mechanism is thought to dominate in most ruthenium-based catalysts.[36,37,80,81] The blue dimer, *cis,cis*-$[(bpy)_2(H_2O)Ru^{III}ORu^{III}(H_2O)(bpy)_2]^{4+}$ (bpy = 2,2′-bipyridine), shown in Figure 9, is perhaps the most widely known complex because it is the first molecular catalyst synthesized for water oxidation. It

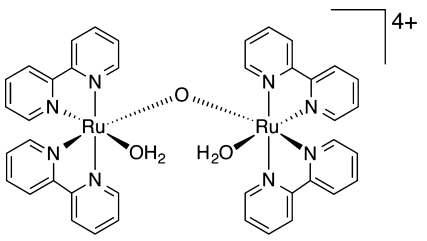

Figure 9. Blue dimer.

dx.doi.org/10.1021/ic5002557 | Inorg. Chem. XXXX, XXX, XXX−XXX

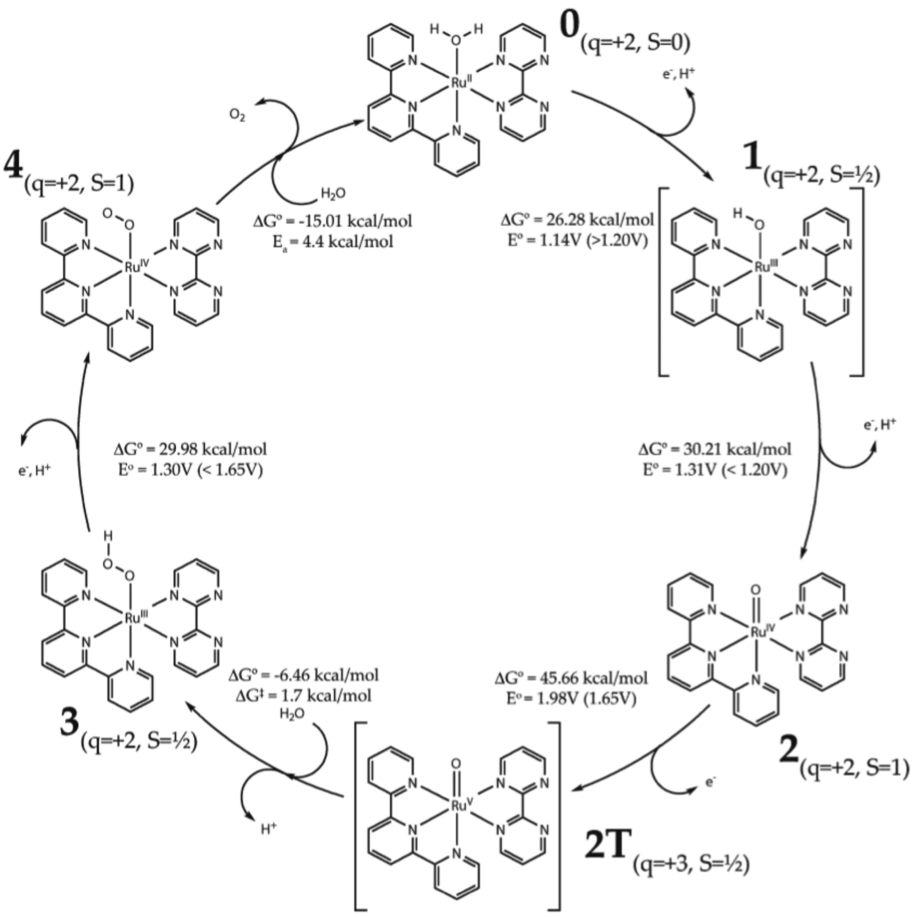

Figure 10. Proposed catalytic cycle with computed thermodynamics with computed redox potentials, where *q* and *S* indicate the charge and spin and species with brackets are not experimentally observed. Experimental redox potentials are reported in parentheses. Reprinted (adapted) with permission from ref 7. Copyright 2010 American Chemical Society.

was suggested theoretically[36] and experimentally[82] that stepwise PCET oxidation of the blue dimer leads to $[(O)Ru^{V}ORu^{V}(O)]^{4+}$ as the catalytically active form, which then rapidly rearranges to a peroxide intermediate, $[(OOH)Ru^{IV}ORu^{IV}(O)]^{4+}$, upon O−O bond formation. Although it is a bimetal complex, the proposed mechanism is of the acid-base type instead of the direct-coupling type: one metal center plays an essential role, while the function of the other metal center is only assistive. Although there have been many two-center ruthenium complexes synthesized as water oxidation catalysts with the blue dimer in mind, the prevalence of one center throughout the catalytic cycle of the blue dimer led Concepcion et al. to propose novel ruthenium monomers $[Ru(tpy)(bpm)(OH_2)]^{2+}$ and $[Ru(tpy)(bpz)(OH_2)]^{2+}$ (tpy = 2,2′:6′,2″-terpyridine; bpm = 2,2′-bipyrimidine; bpz = 2,2′-bipyrazine), both of which involve an important intermediate, $[Ru^{V}(O)]^{3+}$.[6] The proposed acid-base mechanism for these monomers is shown in Figure 10 with some minor modifications.

In a previous study,[7] we have assessed this mechanism using DFT with QM/MM for explicit solvent sampling in order to achieve high accuracy in computing the redox potentials. Thermodynamic information is especially important to identify a plausible reaction path as well as the RLS. The computed redox potentials are listed in Figure 10.

In this mechanism, oxidation of $[Ru^{II}(OH_2)]^{2+}$ (**0** in Figure 10) proceeds to $[Ru^{IV}(O)]^{2+}$ (**2**) directly through two PCET reactions, i.e., loss of both protons and electrons. There is a kinetic intermediate of ruthenium(III) (**1**), which is experimentally unstable and not observable. The DFT results unfortunately gave the incorrect ordering of the potential ($E°$ = 1.14 V for the first PCET and $E°$ = 1.31 V for the second), although the agreement with the experimental value of 1.20 V is noteworthy.

Oxidation of **2** to $[Ru^{V}(O)]^{3+}$ (**2T**) takes place without proton transfer at $E°$ = 1.65 V and pH 1 experimentally. DFT with QM/MM predicted a redox potential of 1.98 V, which disagrees with the experiment by more than 0.3 V. This key intermediate, like in the blue dimer, is then nucleophilically attacked by water to become a peroxide, $[Ru^{III}OOH]^{2+}$ (**3**), which is similar to the proposed step for O−O bond formation in photosystem II.[21] While the experiments by Polyansky et al. suggested the same pathway involving $Ru^{V}(O)$ for a similar but different monomer at standard conditions, it was also proposed that at high alkalinity an alternative concerted PCET governs the step **2** → **3** instead, although its exact mechanism is not yet known.[83] The theoretical finding in ref 7 was that any $Ru^{IV}(O)$ complex with an O−O bond was structurally unstable, indicating that higher oxidation states, i.e., $Ru^{V}(O)$, are needed. It is also worth mentioning that any bimolecular O−O-bonded cluster $[Ru^{IV/V}(O)-(O)Ru^{IV/V}]$ theoretically lies at a much higher energy state than the corresponding pair of monomers, thoroughly eliminating the possibility of a direct-coupling mechanism for this system. Concepcion et al. reported that this O−O bond formation step by the nucleophilic attack of water

dx.doi.org/10.1021/ic5002557 | Inorg. Chem. XXXX, XXX, XXX−XXX

is much more rapid in the blue dimer than in the monomers. It was suggested that the reason for this is that, in the blue dimer, one $Ru^{V}(O)$ forms a bond with OH, while the other $Ru^{V}(O)$ piece holds residual hydrogen[36,61] in a concerted electron−proton transfer (Figure 11), avoiding formation of a high

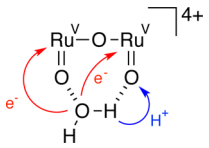

Figure 11. Concerted electron−proton transfer in formation of the O−O bond in the blue dimer.

energy state of $Ru-O-OH_2$. On the other hand, for one-center complexes, Mulliken population analysis indicated that only a proton is transferred to the solvent during this step (**2T** → **3** in Figure 10), albeit with low activation energy (1.7 kcal/mol at the transition state).

Intermediate **3** is further oxidized to $[Ru^{IV}OO]^{2+}$ (**4**) through spontaneous PCET. While **3** is not observed in the experiment, evidence for the existence of **3** is provided both by cyclic voltammetry experiments and by the absorption spectrum calculated by time-dependent DFT, which agrees well with the experimental absorption spectrum of its analogue.[61] Computationally, we also found no barrier between **3** and **4**: all 40 sampled configurations of **3** with the explicit solvent effect immediately deprotonated to give **4**, in agreement with experiments.

The catalytic cycle is completed by the step **4** → **0**, where O_2 is replaced by water. We found a small barrier of 4.4 kcal/mol but with a large downhill driving force of −15.0 kcal/mol toward **0**.

In ref 7, we also investigated the reaction mechanism of two-center catalyst $[(bpy)(H_2O)Ru^{II}(tpy\text{-}DBF\text{-}tpy)Ru^{II}(OH_2)(bpy)]^{4+}$ (DBF = dibenzofuran). Although explicit solvent effects had to be omitted because of the prohibitively large system size, the calculations showed that an acid-base mechanism is still preferable compared to a direct-coupling mechanism because the latter has a large steric and electrostatic barrier, which rules it out as mentioned above. Interestingly, the O−O bond formation step in the two-center case consistently resembles that in the one-center case: one of the metal centers is oxidized to Ru^{V}, i.e., $[(O)Ru^{IV}Ru^{V}(O)]^{5+}$, followed by nucleophilic attack of a water molecule to form, again, a peroxide, $[(O)Ru^{IV}Ru^{III}(OOH)]^{4+}$. That the mechanism is of the acid-base type means that the main role of the other ruthenium center is to assist the oxidation steps at the active center, similarly to the blue dimer. This result is also consistent with other DFT studies on ruthenium complexes.[36,37]

It should also be pointed out that, when computing these bimetal systems, one has to be careful about self interaction error in DFT:[84,85] conventional DFT functionals delocalize the electron distribution as $[(O)Ru^{4.5}Ru^{4.5}(O)]^{5+}$ for this complex instead of $[(O)Ru^{IV}Ru^{V}(O)]^{5+}$. This result is unphysical given that two metal centers are weakly interacting. Therefore, in order to obtain the highly oxidized ruthenium(V) center, we have utilized constrained DFT,[86] allowing us to remove this artificial effect.

Direct-Coupling Mechanism. Few studies have conclusively pointed to a direct-coupling mechanism that can energetically compete. Nevertheless, several studies suggest that a direct-coupling mechanism may be at play for these catalysts. Using DFT as well as wavefunction theory, Muckerman et al.[87] proposed a direct-coupling mechanism of a novel binuclear ruthenium complex, $[Ru_2(OH)_2(3,6\text{-}Bu_2Q)_2(btpyan)](SbF_6)_2$ [3,6-Bu_2Q = 3,6-di*tert*-butyl-1,2-benzoquinone; btpyan = 1,8-bis(2,2′:6′,2″-terpyrid-4′-yl)-anthracene] prepared by Tanaka and co-workers.[88] As shown in Figure 12, the so-called "Tanaka catalyst" has an interesting

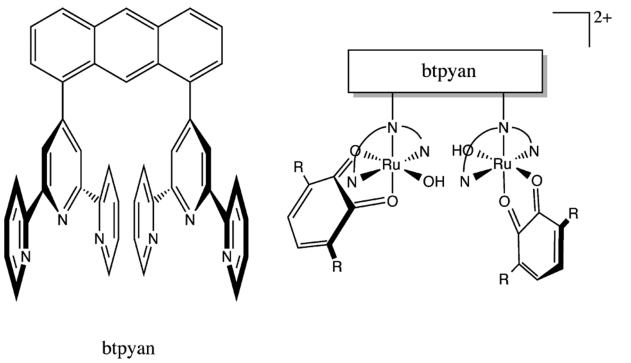

Figure 12. Binuclear Tanaka catalyst.

structure, which has an OH group on each ruthenium center in close enough proximity to make an O−O bond. Theoretical calculations revealed that the initial spin state of the species is a singlet, which are consistent with experiment. The catalyst becomes a triplet by an appropriate intersystem crossing and remains a triplet for the rest of the catalytic cycle. It is interesting that, contrary to many other organometallic catalysts, DFT spin-density analysis showed that the Tanaka catalyst involves oxidation of quinone (to semiquinone and catecholate) exclusively but *not* of the metal centers, which remain ruthenium(II) throughout the entire catalytic cycle. Hence, the ruthenium centers play the role of mediating the intramolecular electron transfer from a water molecule and the quinone ligands.

Because the purpose of that study was to clarify the electronic properties of a large number of possible intermediate species, these calculations were done in the gas phase, treating neither implicit nor explicit solvent effects. The study showed that, even without appropriate solvent effects, the geometrical mechanics of the catalyst is consistent with experimental observations. However, the detailed energetics and kinetics remain unclear from the computational side, and as discussed above, this information is necessary in order to gain deeper insight into the catalytic mechanisms.

As we have seen, redox energetics are highly important for quantitative analysis of reaction mechanisms, and this is by no means limited to ruthenium catalysts. State-of-the-art DFT methodologies have proven beneficial in predicting the thermodynamics, kinetics, and electronic structures of water-splitting catalysts, which has, in turn, allowed us to identify reaction pathways and predict mechanisms. We have also seen the need for the further development of computational methods that are both accurate and cost-effective, given that the experimental and computational results can contradict occasionally. We note that all of the water-splitting catalysts should be categorized into either the acid-base or direct-coupling type. As we showed above, with the help of both experimental and computational studies, one can learn which type is more dominant by investigating each reaction path, the

dx.doi.org/10.1021/ic5002557 | *Inorg. Chem.* XXXX, XXX, XXX−XXX

associated intermediates, and sometimes the transition states. Especially important is how O_2 is formed and released because in many cases it is the key step in water-splitting catalysts. Although many catalysts are nonstoichiometric bulk solid-state materials (e.g., perovskites) rather than molecules and are thus computationally very demanding, mechanistic studies on model molecular catalysts can be very valuable for understanding similar mechanisms in bulk catalysts to answer these questions. Detailed thermodynamics that DFT with QM/MM has to offer can provide fruitful information not only to support experimental results but also to propose mechanisms, and it allows us to further investigate more appropriate ligands for catalytic optimization.

CONCLUSIONS

Artificial water oxidation catalysis is poised to become a commercially significant technology in the near future. A detailed understanding of the structure and reactivity of candidate catalysts will play an essential role in further catalyst design and optimization. In this Forum Article, we have discussed the current state-of-the-art methods in electronic structure calculations of artificial water oxidation catalysts, with an emphasis on how DFT is used to explore reactivity trends and underlying mechanisms. DFT thermochemistry can be employed to quantify chemical descriptors of reactivity, and these descriptors reproduce experimentally observed "volcano plots" describing the dependence of the catalytic activity on the constituent transition metal. The proper incorporation of solvent effects remains a challenge, but polarizable QM/MM and full DFT models of the surrounding water provided insight into the sequence of PCET events in the catalytic cycle of the CoPi water oxidation catalyst. Detailed QM/MM studies of one- and two-center ruthenium catalysts allowed us to determine the relative plausibility of acid-base and direct-coupling mechanisms in these systems.

The ability of theory and computation to address the mechanism of water oxidation catalysis is largely tied to developments in DFT and other electronic structure theories. Current shortcomings relevant to the artificial water oxidation problem include the treatment of dispersion effects, reaction barrier heights, and the underlying issue of self-interaction error. All of these areas are very active topics of research, and there is good reason to expect steady improvement in the accuracy of DFT models for water oxidation catalysts in the coming years.

Efforts to harness DFT models of structure and reactivity for computational screening of materials are already underway,[89−91] and water oxidation catalysis is a natural target to include in such studies.[23] Through the combination of electronic structure calculations with cheminformatic approaches, the necessary machinery for high-throughput screening of candidate materials is within reach and will likely produce useful leads in the near future. However, neither cheminformatic approaches nor mechanistic studies will attain their full potential without vigorous experimental collaboration. Input from experiments will help refine informatic approaches and will continue to push the limits of our mechanistic models. Together, theoretical and experimental mechanistic studies will continue to drive advances in artificial water oxidation catalysis.

ASSOCIATED CONTENT

Supporting Information

Computational procedures and model selection criteria. This material is available free of charge via the Internet at http://pubs.acs.org.

AUTHOR INFORMATION

Corresponding Author

*E-mail: tvan@mit.edu.

Notes

The authors declare no competing financial interest.

ACKNOWLEDGMENTS

The work of M.G.M., T.T., and A.M. on homobimetallic clusters was supported primarily by the MIT MRSEC through the MRSEC Program of the National Science Foundation under Award DMR-0819762. The work of L.-P.W. and T.K. on the CoPi and ruthenium catalysts was funded through the ENI-MIT solar frontiers center. M.G.M. thanks the NSF for a GRFP fellowship and Prof. Yogesh Surendranath for helpful discussions regarding the relationship of the thermodynamics of the OER to its likely mechanism. The authors thank Profs. Jens Nørskov, Jan Rossmeisl, and Yang Shao-Horn for helpful discussions and figure reproduction permission.

REFERENCES

(1) Brédas, J.; Deljonne, D.; Coropceanu, V.; Jérôme, C. *Chem. Rev.* **2004**, *104*, 4971−5004.
(2) Grätzel, M. *Inorg. Chem.* **2005**, *44*, 6841−6851.
(3) Wong, K. V.; Perilla, N.; Paddon, A. *J. Energy Resour. Technol.* **2013**, *136*, 014001.
(4) Kudo, A.; Miseki, Y. *Chem. Soc. Rev.* **2009**, *38*, 253−278.
(5) Nocera, D. G. *Acc. Chem. Res.* **2012**, *45*, 767−776.
(6) Concepcion, J. J.; Jurss, J. W.; Templeton, J. L.; Meyer, T. J. *J. Am. Chem. Soc.* **2008**, *130*, 16462−16463.
(7) Wang, L.-P.; Wu, Q.; Van Voorhis, T. *Inorg. Chem.* **2010**, *49*, 4543−4553.
(8) Kanan, M. W.; Nocera, D. G. *Science* **2008**, *321*, 1072−1075.
(9) Suntivich, J.; May, K. J.; Gasteiger, H. A.; Goodenough, J. B.; Shao-Horn, Y. *Science* **2011**, *334*, 1383−1385.
(10) Wang, Y.; Cheng, H.-P. *J. Phys. Chem. C* **2013**, *117*, 2106−2112.
(11) Risch, M.; Klingan, K.; Ringleb, F.; Chernev, P.; Zaharieva, I.; Fischer, A.; Dau, H. *ChemSusChem* **2012**, *5*, 542−549.
(12) Siegbahn, P. E. M. *Acc. Chem. Res.* **2009**, *42*, 1871−1880.
(13) Lloret Fillol, J.; Codolá, Z.; Garcia-Bosch, I.; Gómez, L.; Pla, J. J.; Costas, M. *Nat. Chem.* **2011**, *3*, 807−813.
(14) Joya, K. S.; de Groot, H. J. *Int. J. Hydrogen Energy* **2012**, *37*, 8787−8799.
(15) Tagore, R.; Crabtree, R. H.; Brudvig, G. W. *Inorg. Chem.* **2008**, *47*, 1815−1823.
(16) Wang, L.-P.; Van Voorhis, T. *J. Phys. Chem. Lett.* **2011**, *2*, 2200−2204.
(17) Surendranath, Y.; Kanan, M. W.; Nocera, D. G. *J. Am. Chem. Soc.* **2010**, *132*, 16501−16509.
(18) Bediako, D. K.; Surendranath, Y.; Nocera, D. G. *J. Am. Chem. Soc.* **2013**, *135*, 3662−3674.
(19) Walter, M. G.; Warren, E. L.; McKone, J. R.; Boettcher, S. W.; Mi, Q.; Santori, E. A.; Lewis, N. S. *Chem. Rev.* **2010**, *110*, 6446−6473.
(20) Imanishi, A.; Okamura, T.; Ohashi, N.; Nakamura, R.; Nakato, Y. *J. Am. Chem. Soc.* **2007**, *129*, 11569−11578.
(21) McEvoy, J. P.; Gascon, J. A.; Batista, V. S.; Brudvig, G. W. *Photochem. Photobiol. Sci.* **2005**, *4*, 940−949.
(22) McEvoy, J. P.; Brudvig, G. W. *Chem. Rev.* **2006**, *106*, 4455−4483.
(23) Greeley, J.; Jaramillo, T. F.; Bonde, J.; Chorkendorff, I. B.; Nørskov, J. K. *Nat. Mater.* **2006**, *5*, 909−913.

dx.doi.org/10.1021/ic5002557 | *Inorg. Chem.* XXXX, XXX, XXX−XXX

(24) Sabatier, P. *Ber. Dtsch. Chem. Ges.* **1911**, *44*, 1984−2001.
(25) Nørskov, J. K.; Bligaard, T.; Rossmeisl, J.; Christensen, C. H. *Nat. Chem.* **2009**, *1*, 37−46.
(26) Mayer, J. M. *Annu. Rev. Phys. Chem.* **2004**, *55*, 363−390.
(27) Hammes-Schiffer, S. *Acc. Chem. Res.* **2009**, *42*, 1881−1889.
(28) Pople, J. A.; Head-Gordon, M.; Fox, D. J.; Raghavachari, K.; Curtiss, L. A. *J. Chem. Phys.* **1989**, *90*, 5622.
(29) Curtiss, L. A.; Raghavachari, K.; Redfern, P. C.; Pople, J. A. *J. Chem. Phys.* **1997**, *106*, 1063.
(30) Hawkins, G. D.; Cramer, C. J.; Truhlar, D. G. *J. Phys. Chem. B* **1998**, *5639*, 3257−3271.
(31) Rizzo, R. C.; Aynechi, T.; Case, D. A.; Kuntz, I. D. *J. Chem. Theory Comput.* **2006**, *2*, 128−139.
(32) Takano, Y.; Houk, K. *J. Chem. Theory Comput.* **2005**, *1*, 70−77.
(33) Cramer, C. J.; Truhlar, D. G. *Acc. Chem. Res.* **2008**, *41*, 760−768.
(34) Wang, L.-P.; Van Voorhis, T. *J. Chem. Theory Comput.* **2012**, *8*, 610−617.
(35) Yang, X. F.; Baik, M. H. *J. Am. Chem. Soc.* **2004**, *126*, 13222−13223.
(36) Yang, X. F.; Baik, M. H. *J. Am. Chem. Soc.* **2006**, *128*, 7476−7485.
(37) Yang, X. F.; Baik, M. H. *J. Am. Chem. Soc.* **2008**, *130*, 16231−16240.
(38) Rossmeisl, J.; Logadottir, A.; Nørskov, J. K. *Chem. Phys.* **2005**, *319*, 178−184.
(39) Nørskov, J. K.; Rossmeisl, J.; Logadottir, A.; Lindqvist, L.; Kitchin, J. R.; Bligaard, T.; Jónsson, H. *J. Phys. Chem. B* **2004**, *108*, 17886−17892.
(40) Curtiss, L. A.; Raghavachari, K.; Trucks, G. W.; Pople, J. A. *J. Chem. Phys.* **1991**, *94*, 7221.
(41) Jiménez-Hoyos, C. A.; Janesko, B. G.; Scuseria, G. E. *Phys. Chem. Chem. Phys.* **2008**, *10*, 6621−6629.
(42) Chase, M. W. J. *NIST-JANAF Thermochemical Tables*, 4th ed.; American Institute of Physics: New York, 1998.
(43) Harvey, J. N. *Struct. Bonding (Berlin)* **2004**, *112*, 151−183.
(44) Cramer, C. J.; Truhlar, D. G. *Phys. Chem. Chem. Phys.* **2009**, *11*, 10757−816.
(45) Oberhofer, H.; Reuter, K. *J. Chem. Phys.* **2013**, *139*, 044710.
(46) Swart, M. *Inorg. Chim. Acta* **2007**, *360*, 179−189.
(47) Hughes, T. F.; Friesner, R. A. *J. Chem. Theory Comput.* **2012**, *8*, 442−459.
(48) Klamt, A.; Mennucci, B.; Tomasi, J.; Barone, V.; Curutchet, C.; Orozco, M.; Luque, F. J. *Acc. Chem. Res.* **2009**, *42*, 489−492.
(49) Palascak, M. W.; Shields, G. C. *J. Phys. Chem. A* **2004**, *108*, 3692−3694.
(50) Camaioni, D. M.; Schwerdtfeger, C. A. *J. Phys. Chem. A* **2005**, *109*, 10795−10797.
(51) Kelly, C. P.; Cramer, C. J.; Truhlar, D. G. *J. Phys. Chem. B* **2006**, *110*, 16066−16081.
(52) Konezny, S. J.; Doherty, M. D.; Luca, O. R.; Crabtree, R. H.; Soloveichik, G. L.; Batista, V. S. *J. Phys. Chem. C* **2012**, *116*, 6349−6356.
(53) Vojvodic, A.; Nørskov, J. K. *Science* **2011**, *334*, 1355−1356.
(54) Man, I. C.; Su, H.-Y.; Calle-Vallejo, F.; Hansen, H. A.; Martínez, J. I.; Inoglu, N. G.; Kitchin, J.; Jaramillo, T. F.; Nørskov, J. K.; Rossmeisl, J. *ChemCatChem* **2011**, *3*, 1159−1165.
(55) Bork, N.; Bonanos, N.; Rossmeisl, J.; Vegge, T. *Phys. Rev. B* **2010**, *82*, 1−6.
(56) Koper, M. T. *J. Electroanal. Chem.* **2011**, *660*, 254−260.
(57) Suntivich, J.; Gasteiger, H. A.; Yabuuchi, N.; Nakanishi, H.; Goodenough, J. B.; Shao-Horn, Y. *Nat. Chem.* **2011**, *3*, 546−550.
(58) Liu, X.; Wang, F. *Coord. Chem. Rev.* **2012**, *256*, 1115−1136.
(59) Betley, T. A.; Wu, Q.; Van Voorhis, T.; Nocera, D. G. *Inorg. Chem.* **2008**, *47*, 1849−1861.
(60) Bockris, J. O.; Otagawa, T. *J. Phys. Chem.* **1983**, *87*, 2960−2971.
(61) Concepcion, J. J.; Tsai, M.-K.; Muckerman, J. T.; Meyer, T. J. *J. Am. Chem. Soc.* **2010**, *132*, 1545−1557.
(62) Yang, X.; Hall, M. B. *J. Am. Chem. Soc.* **2010**, *132*, 120−130.
(63) Kanan, M. W.; Surendranath, Y.; Nocera, D. G. *Chem. Soc. Rev.* **2009**, *38*, 109−114.
(64) Du, P.; Kokhan, O.; Chapman, K. W.; Chupas, P. J.; Tiede, D. M. *J. Am. Chem. Soc.* **2012**, *134*, 11096−11099.
(65) Kanan, M. W.; Yano, J.; Surendranath, Y.; Dinca, M.; Yachandra, V. K.; Nocera, D. G. *J. Am. Chem. Soc.* **2010**, *132*, 13692−13701.
(66) Li, X.; Siegbahn, P. E. M. *J. Am. Chem. Soc.* **2013**, *135*, 13804−13813.
(67) Mattioli, G.; Risch, M.; Bonapasta, A. A.; Dau, H.; Guidoni, L. *Phys. Chem. Chem. Phys.* **2011**, *13*, 15437−15441.
(68) Zeng, X. C.; Hu, H.; Hu, X. Q.; Yang, W. *J. Chem. Phys.* **2009**, *130*, 164111.
(69) Chiorescu, I.; Deubel, D. V.; Arion, V. B.; Keppler, B. K. *J. Chem. Theory Comput.* **2008**, *4*, 499−506.
(70) Steindal, A. H.; Ruud, K.; Frediani, L.; Aidas, K.; Kongsted, J. *J. Phys. Chem. B* **2011**, *115*, 3027−3037.
(71) Stewart, J. J. P. *Reviews in Computational Chemistry*; John Wiley and Sons, Inc.: New York, 2007; pp 45−81.
(72) Lamoureux, G.; Roux, B. *J. Chem. Phys.* **2003**, *119*, 3025−3039.
(73) Hirata, F.; Rossky, P. J. *Chem. Phys. Lett.* **1981**, *83*, 329−334.
(74) Ten-no, S.; Hirata, F.; Kato, S. *Chem. Phys. Lett.* **1993**, *214*, 391−396.
(75) Tannor, D. J.; Marten, B.; Murphy, R.; Friesner, R. A.; Sitkoff, D.; Nicholls, A.; Honig, B.; Ringnalda, M.; Goddard, W. A., III *J. Am. Chem. Soc.* **1994**, *116*, 11875−11882.
(76) Becke, A. *J. Chem. Phys.* **1993**, *98*, 5648.
(77) Klamt, A.; Schuurmann, G. *J. Chem. Soc., Perkin Trans. 2* **1993**, *2*, 799−805.
(78) Mattioli, G.; Giannozzi, P.; Bonapasta, A. A.; Guidoni, L. *J. Am. Chem. Soc.* **2013**, *135*, 15353−15363.
(79) Neumann, M. *J. Chem. Phys.* **1986**, *85*, 1567.
(80) Hurst, J. K.; Zhou, J. Z.; Lei, Y. B. *Inorg. Chem.* **1992**, *31*, 1010−1017.
(81) Zong, R.; Thummel, R. P. *J. Am. Chem. Soc.* **2005**, *127*, 12802−12803.
(82) Liu, F.; Concepcion, J.; Jurss, J. W.; Cardolaccia, T.; Templeton, J. L.; Meyer, T. *Inorg. Chem.* **2008**, *47*, 1727−1752.
(83) Polyansky, D. E.; Muckerman, J. T.; Rochford, J.; Zong, R.; Thummel, R. P.; Fujita, E. *J. Am. Chem. Soc.* **2011**, *133*, 14649−14665.
(84) Perdew, J. P.; Zunger, A. *Phys. Rev. B* **1981**, *23*, 5048−5079.
(85) Wu, Q.; Van Voorhis, T. *J. Phys. Chem. A* **2006**, *110*, 9212−9218.
(86) Wu, Q.; Van Voorhis, T. *Phys. Rev. A* **2005**, *72*, 024502.
(87) Muckerman, J. T.; Polyansky, D. E.; Wada, T.; Tanaka, K.; Fujita, E. *Inorg. Chem.* **2008**, *47*, 1787−1802.
(88) Wada, T.; Tsuge, K.; Tanaka, K. *Inorg. Chem.* **2001**, *40*, 329−337.
(89) Hachmann, J.; Olivares-Amaya, R.; Atahan-Evrenk, S.; Amador-Bedolla, C.; Sanchez-Carrera, R.; Gold-Parker, A.; Vogt, L.; Brockway, A. M.; Aspuru-Guzik, A. *J. Phys. Chem. Lett.* **2011**, *2*, 2241−2251.
(90) Hautier, G.; Fischer, C. C.; Jain, A.; Mueller, T.; Ceder, G. *Chem. Mater.* **2010**, *22*, 3762−3767.
(91) Kanal, I. Y.; Owens, S. G.; Bechtel, J. S.; Hutchison, G. R. *J. Phys. Chem. Lett.* **2013**, *4*, 1613−1623.